

Article

A One-Dimensional Cu(I) Coordination Polymer with Optical Sensing of Oxygen and Temperature

Wan-Tao Chen [†] , Chen-Hui Li [†], Wan-Qing Zhou, Jing-Tao Huang, Jia-Wen Ye ^{*†}  and Ling Chen ^{*}

School of Biotechnology and Health Sciences, Wuyi University, Jiangmen 529000, China

^{*} Correspondence: wyuchemyjw@126.com (J.-W.Y.); wyuclm@126.com (L.C.)[†] These authors contributed equally to this work.

Abstract: Due to their tight structures, it is usually difficult for one-dimensional (1D) coordination polymers (CPs) to form permanent pores unless 2D and 3D topologies are formed via supramolecular interactions, so studies in the field of oxygen sensing on 1D CPs are rarely reported. Here, we report a 1D Cu(I) cluster-based CP with dual sensing characteristics for temperature and oxygen. Even if the porosity is only 6.6%, the quenching rate of this CP reaches 98.4% with 1 bar O₂ at room temperature. Its luminescence intensity exhibits a unique thermal “quenching, then activating” behavior during monotonic variations in temperature.

Keywords: coordination polymer; luminescent thermometer; optical oxygen sensing



Citation: Chen, W.-T.; Li, C.-H.; Zhou, W.-Q.; Huang, J.-T.; Ye, J.-W.; Chen, L. A One-Dimensional Cu(I) Coordination Polymer with Optical Sensing of Oxygen and Temperature. *Inorganics* **2022**, *10*, 253. <https://doi.org/10.3390/inorganics10120253>

Academic Editors: Si-Yang Liu and Yuzhi Xu

Received: 7 November 2022

Accepted: 8 December 2022

Published: 10 December 2022

Publisher's Note: MDPI stays neutral with regard to jurisdictional claims in published maps and institutional affiliations.



Copyright: © 2022 by the authors. Licensee MDPI, Basel, Switzerland. This article is an open access article distributed under the terms and conditions of the Creative Commons Attribution (CC BY) license (<https://creativecommons.org/licenses/by/4.0/>).

1. Introduction

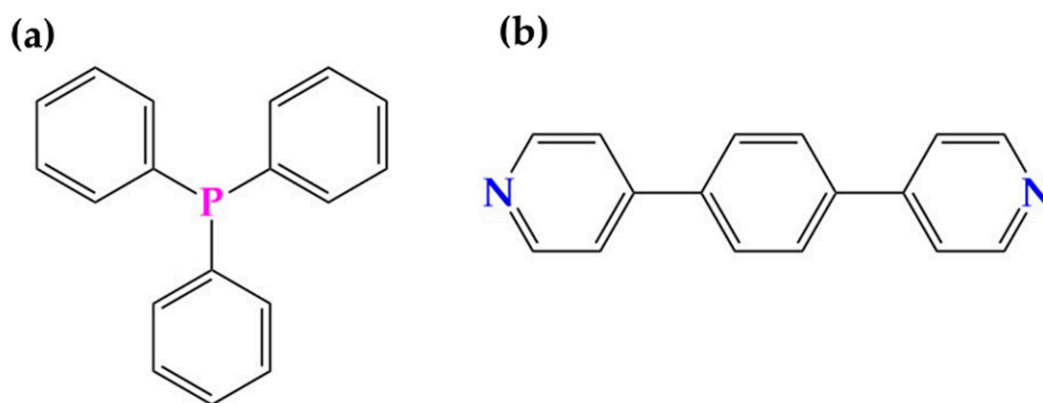
Luminescent coordination polymers (CPs) have been extensively studied over the last few decades due to their great potential for white-light illumination [1] and sensing [2,3] and their long afterglow [4]. Oxygen and temperature sensing plays essential roles in industrial production, grain storage, and aerospace research [5,6]. Unfortunately, one-dimensional (1D) CPs are mainly closely packed structures, which makes it hard to form pores and is not conducive to their application in fluorescence sensing [7]. Upon the lengthening of the bridging ligand, the interactions between adjacent chains can be effectively reduced, which helps to create a relatively loose structure [8] and to obtain CPs with a small number of channels. Compared with other reported CPs, metal-cluster-based CPs are more susceptible to environmental stimulation due to the existence of various transition modes, such as the metal-centered (MC) transition [9], cluster-centered (CC) transition [10], metal-to-ligand charge transfer (MLCT) [11], halogen-to-metal charge transfer (XLCT) [12,13], and metal–metal-to-ligand charge transfer (MMLCT) [14], so their luminescence is prone to shifting, being enhanced, or being quenched under solvents, oxygen, pressure, and other stimuli [15–22]. However, 1D CPs are usually close-packing, and porous 1D Cu(I) or Cu(I) cluster-based CPs are rarely reported [23,24], which limits their applications in oxygen and solvent sensing [25–29]. The luminescence of most organic and coordination compounds is inclined to be quenched when the temperature rises due to the increase in the thermal vibration [30,31].

In this work, we report a 1D [Cu₂I₂] cluster-based CP (donated as **1**), which showed a modicum of inherent channels with a porosity of 6.6%. The luminescence of **1** was assigned to the mixed XLCT and MLCT transition with a maximum emission wavelength (λ_{em}) at 542 nm, and it was sensitive to both oxygen and temperature. In an oxygen environment, the luminescence of **1** was effectively quenched, and the quenching rate reached 98.4% with 1 bar O₂ and room temperature. This revealed that the 1D CP could still maintain good oxygen sensing capabilities, although the porosity was not high. Additionally, when the temperature was decreased, the luminescence of **1** showed a blue-shifting tendency. The luminescent intensity decreased and then gradually increased in the heating process.

2. Results and Discussion

2.1. Preparation of $[\text{Cu}_2\text{I}_2(\text{TPP})_2(\text{BPB})]\cdot\text{CH}_3\text{OH}$ (**1·g**)

A mixture of triphenylphosphine (TPP, 0.2 mmol, 53 mg), CuI (0.2 mmol, 38 mg), acetonitrile (10 mL), and BPB (0.1 mmol, 23 mg) was placed in a glass vial (20 mL) and then stirred for about 10 min until it was well mixed. After 1 week, the yellow crystals were observed, collected, and then immersed in methanol for two days. The crystals were washed with fresh methanol three times, and **1·g** was obtained with a yield of 70% (about 82 mg). After drying under a vacuum at 60 °C for one day, compound **1** without a guest was obtained. The ligand structures are shown in Figure 1. An elemental analysis and FTIR results are shown in Table S1 and Figure S1, respectively.



Triphenylphosphine (TPP) 1,4-bis(pyrid-4-yl)benzene (BPB)

Figure 1. Molecular structures of (a) TPP and (b) BPB.

2.2. Crystal Structures of **1** and **1·g**

The activated **1** is isostructural with **1·g**; the difference lies in if they are with (**1·g**) or without (**1**) guest molecules. Here, **1** is taken as an example to introduce the structure. Single-crystal X-ray diffraction (SCXRD) showed that **1** crystallized in a triclinic $P\bar{1}$ space group, and the smallest asymmetric unit in it was composed of one CuI, one TPP, and half of a BPB (Figure 2a). The Cu(I) in the $[\text{Cu}_2\text{I}_2]$ nodes coordinated with the N atoms of BPB, and then infinitely connected to form a 1D chain (Figure 2b). TPP was coordinated with Cu(I) ion and was located between the adjacent chains. The three-dimensional (3D) supramolecular structure was formed by infinite parallel stacking of 1D chains (Figure 2c). Moreover, though the TPP ligand interpenetrated into the vicinity of the bridging ligand of the adjacent chain, it could not fill the whole area that was surrounded by two TPP ligands, one bridging ligand, and two $[\text{Cu}_2\text{I}_2]$ clusters, thus leaving a small cavity. The porosity of **1** increased by 6.6% after removing the guest (Figure 2d). For more detailed crystal data, please see the Supplementary Materials (Table S2). By comparison, it was found that the structure of **1** was consistent with that of **1·g** (Figure S2). The powder X-ray diffraction (PXRD) patterns showed that the crystal phase of the measured sample was consistent with that of the simulated powder (Figure 2e and Figure S3). The thermogravimetric (TG) curve showed that **1** began to decompose at 240 °C (Figure 2f). The TG curve of **1·g** showed a small weight loss before decomposing, which could be assigned to the removal of the CH_3OH guest (Figure 2f).

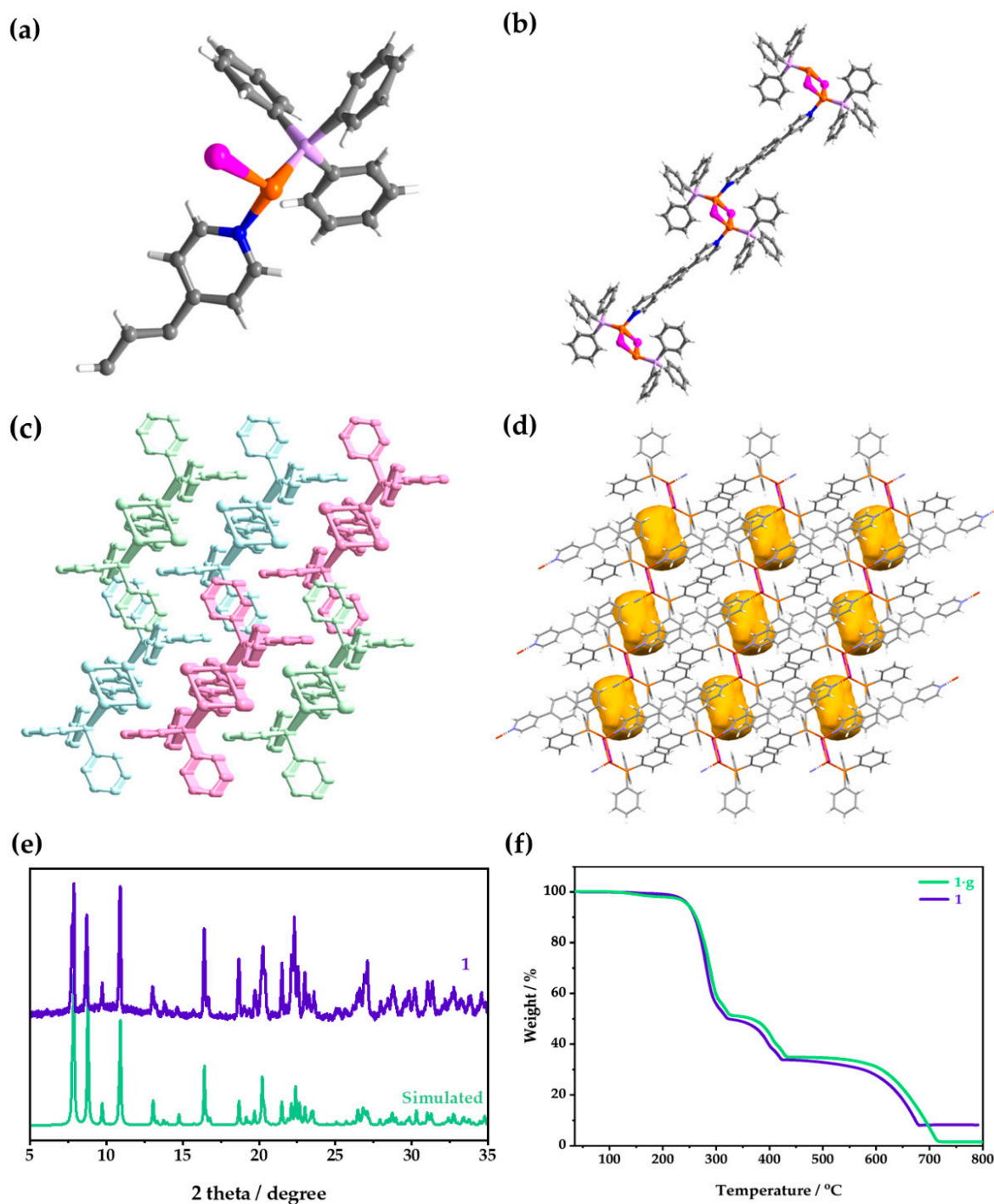


Figure 2. (a) The asymmetric unit, (b) chain structure, (c) 3D supramolecular structure, and (d) channels in the activated structure of **1**. Color codes for (a,b,d): C, gray; H, white; N, blue; P, lavender; Cu, orange; I, pink; Channels, yellow. For (c), different colors are employed to distinguish separate chains, and hydrogen atoms are omitted for clarity. (e) The PXRD patterns of **1** and (f) TG curves of **1** and **1.g**.

2.3. Optical O₂-Sensing Properties

As shown in Figure 3a, **1** exhibited a wide absorption from 200 to 500 nm, with an apparent yellow color that could be attributed to the mixed absorption of the MLCT/XLCT transition [32,33]. Under ambient conditions, λ_{em} was 542 nm (Figure 3b), which could be attributed to the emission of ³MLCT/³XLCT [34,35]. Under changeable-wavelength excitation, **1** showed a similar emission (Figure S4).

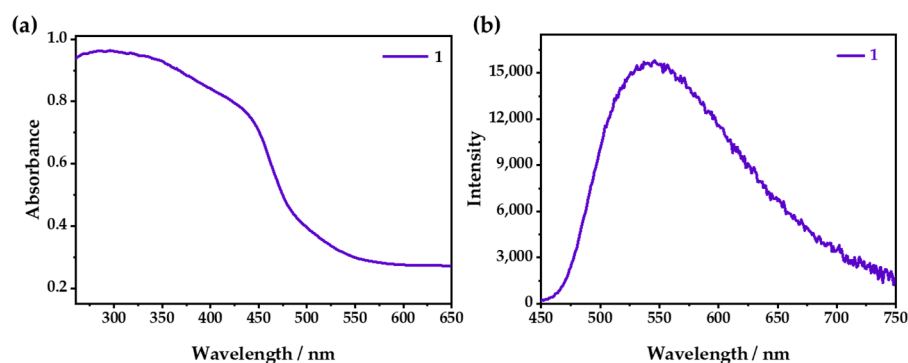


Figure 3. (a) UV-vis absorption and (b) emission spectra of **1** when excited at 365 nm.

The PXRD patterns of **1** and **1·g** were almost the same, indicating that they had very similar structures (Figure S3). However, λ_{em} of **1** was located at 542 nm (Figure S5), and it showed a redshift of 18 nm compared with that of **1·g** ($\lambda_{em} = 524$ nm). The emission of **1** could be quenched due to the tiny number of channels in the structure, which could allow the entry of O_2 . With the increase in oxygen concentration, the luminescence was gradually weakened; furthermore, 98.4% of the luminescence intensity was quenched at 1 bar O_2 (Figure 4a and Figure S6), which was relatively low in comparison with Cu(I) CPs, and this was because of its small cavities [36,37]. However, it was difficult for O_2 to enter the zero-dimensional channels quickly, so it needed a relatively long time to capture O_2 and reach a balance. As shown in Figure 4b, it was demonstrated that the luminescence attenuation was less than 10% after 10 cycles in the O_2 -sensing test. The Stern–Volmer curve was obtained with the fluorescence spectra at different O_2 pressures and fitted according to the equation: $I_0/I = \tau_0/\tau = 1 + K_{SV}P_{O_2}$. The fitting chart exhibited good linearity, and the K_{SV} value was calculated as 62 bar^{-1} (Figure 4c), indicating that **1** had excellent O_2 -sensing performance, with a high sensitivity and good stability. The luminescence of **1·g** could be also quenched by oxygen, but it showed a very low quenching efficiency because the CH_3OH guest occupied the cavities of **1**, which prevented the entry of the oxygen (Figure S7).

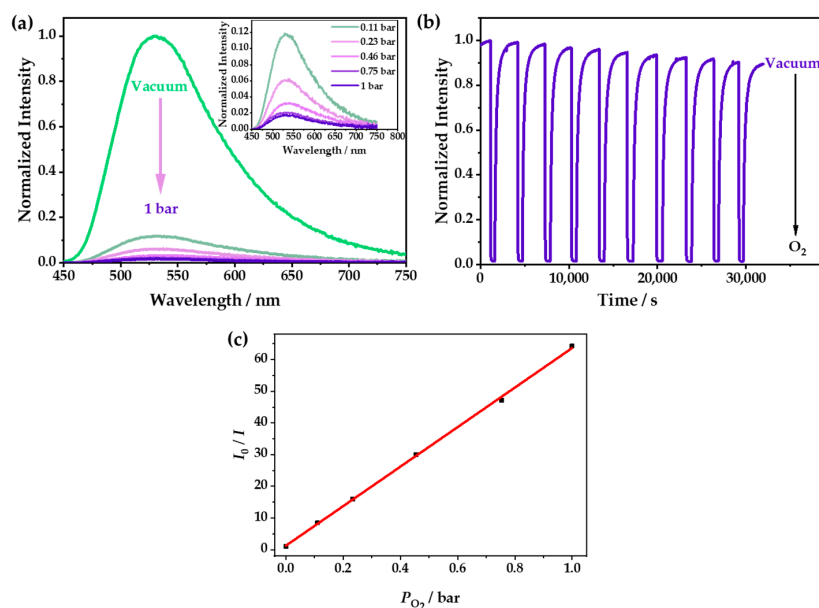


Figure 4. (a) The emission spectra of **1** at different O_2 pressures under an excitation of 365 nm. (b) The time-dependent spectrum of **1** when switching between a vacuum and 1 bar O_2 —excited at 365 nm and detected at 542 nm. (c) The Stern–Volmer plots of **1** at different O_2 pressures—excited at 365 nm and detected at 542 nm.

At 333, 353, and 373 K, the oxygen quenching efficiencies of **1** were 95.0%, 94.0%, and 89.0%, respectively. Interestingly, by studying the time-dependent spectra of **1** when switching between a vacuum and 1 bar O₂, it was found that the response speeds and the optical stabilities could be greatly improved by increasing the temperature (Figure 5). The times that were required to reach the equilibrium at room temperature, 333 K, 353 K, and 373 K were about 2000, 1000, 300, and 200 s, respectively. The response speed could be doubled by increasing the temperature by 20 K. This was probably caused by the flexibility of the windows in **1** and the gradually enhanced gate-opening effect as the temperature increased, which made the oxygen diffuse into the channel more quickly, leading to a faster response speed. Moreover, **1** also showed good reversibility and better photostability after increasing the temperature.

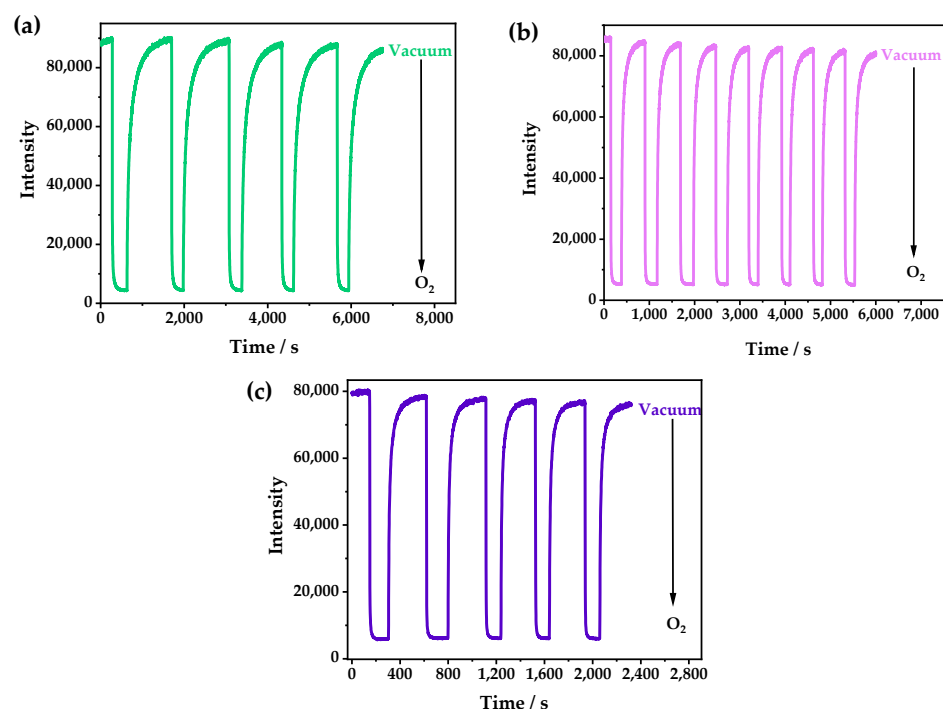


Figure 5. The time-dependent spectra of **1** at (a) 333, (b) 353, and (c) 373 K when switching between a vacuum and 1 bar O₂—excited by 365 nm UV light and detected at 542 nm.

The phosphorescence lifetimes with 1 bar oxygen, air, and vacuum were also measured to further confirm the fluorescence quenching mechanism. It was found that the phosphorescence lifetimes were 0.318, 1.52, and 22 μ s, in 1 bar O₂, air, and a vacuum, respectively (Figure 6 and Table S3), which showed that the luminescence of **1** belonged to a triplet emission, which is easy for oxygen to quench [38].

In addition, the photoluminescence spectra of **1** at different temperatures were investigated. At low temperatures, as the thermal vibration decreased, the emission intensity was significantly increased compared with that at room temperature. At 80 K, the triple emission displayed the multiple peaks located at 508, 546, and 585 nm (Figure 7a), which were considered the fine-structure emissions of BPB. With the increase in the temperature from 80 to 300 K, the integral intensities of the emission spectra displayed a “dropping down and then going up” trend with the excitation at 365 nm. Specifically, from 80 to 240 K, the luminescence intensity gradually decreased, which is usually called thermal quenching (TQ) and is commonly observed in the CPs [39,40]. Notably, when the temperature rose from 240 to 300 K, the luminescence intensity slightly increased, which is unique and may have been caused by the transformation of the ligand or the shortening of the Cu–Cu distance (Figure 7b) [10,41]. However, the luminescence intensity of **1-g** only showed a

simple change upon warming: a monotonic decrease (Figure S8), which was caused by the quenching of the thermal vibration.

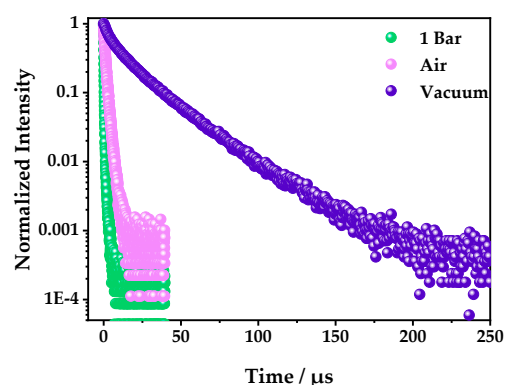


Figure 6. The photoluminescence decay curves of **1** in 1 bar O₂, air, and a vacuum—excited by a 375 nm variable-pulsed laser (VPL) and detected at 542 nm.

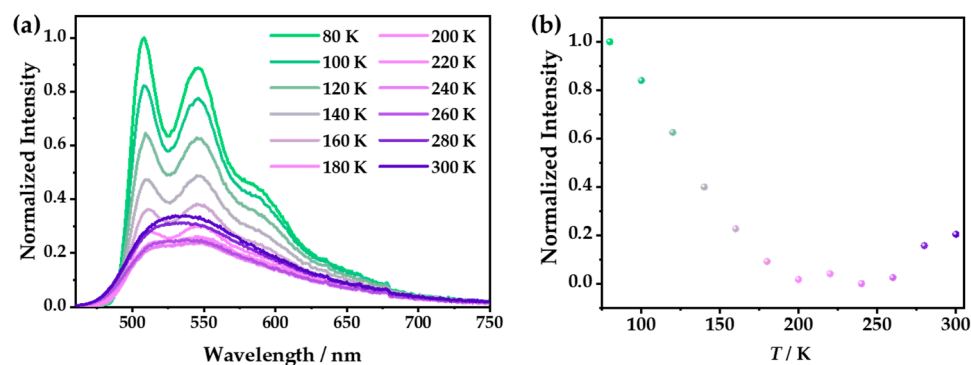


Figure 7. Under excitation at 365 nm, (a) the emission spectra of **1** in the temperature range from 80 to 300 K with an interval of 20 K and (b) the integral intensities of **1** at different temperatures.

3. Materials and Methods

All commercially available reagents and solvents were used as received without further purification. Elemental analyses (C, H, and N) were performed with a Vario EL elemental analyzer (Germany). PXRD patterns were recorded with a Rigaku Mini X-ray powder diffractometer (Japan). UV–vis absorption spectra were recorded on a Shimadzu UV-2600 UV–vis absorption spectrometer (Japan). The TG analyses were performed with a Netzsch STA-409 PC instrument (Germany) with a ramping rate of 10.0 °C min^{−1} under a nitrogen atmosphere. FTIR spectroscopy was measured with a Thermo Fisher Scientific Nicolet iS5 FTIR spectrometer (Massachusetts, USA).

Single-Crystal X-Ray Diffraction. Diffraction data were collected on a Rigaku Xta-LAB single-crystal diffractometer (Japan) by using Cu–K α radiation ($\lambda = 1.54184 \text{ \AA}$). The structures of **1·g** and **1** were solved with the direct methods and refined with the full-matrix least-squares method on F^2 by using the SHELXTL package. Anisotropic thermal parameters were used to refine all non-hydrogen atoms. Hydrogen atoms were generated geometrically. Additional crystallographic information is available in Table S2. CCDC 2215582 contains the supplementary crystallographic data for this paper. These data can be obtained free of charge from the Cambridge Crystallographic Data Centre via www.ccdc.cam.ac.uk/data_request/cif (accessed on 6 November 2022).

Photoluminescence Measurement. The emission spectra were recorded with an Edinburgh FLS1000 fluorescence spectrometer (Britain) equipped with a continuous Xe lamp. All instrument parameters, such as the excitation split, emission split, and scanning speed, were fixed during the in situ measurements. The test temperature was controlled with an Oxford temperature controller. The O₂ responses of photoluminescence were measured in

situ by placing the sample inside an Oxford variable-temperature device with a three-way valve that connected the sample chamber to a vacuum pump and an O₂ cylinder. The lifetime experiments were performed with an Edinburgh FLS1000 fluorescence spectrometer equipped with a VPL at 375 ± 10 nm as the excitation source.

4. Conclusions

In this work, we synthesized a 1D CP based on CuI, TPP, and BPB, which had luminescent temperature and oxygen sensing properties. Although the chains were closely packed in the CP, it still formed zero-dimensional pores that allowed oxygen to enter the channels of the crystal and caused luminescence quenching. The quenching rate of **1** reached 98.4%, which is a very high level compared with that of other reported 1D CPs. By increasing the temperature, the flexible channel could be opened and the O₂ quenching efficiency could be improved. These results can provide a new strategy for controlling and enhancing oxygen luminescence quenching in practical applications. In addition, **1** exhibited a unique thermal “quenching then activating” trend during variations in the temperature, which has barely been observed in luminescent materials, and this mechanism needs to be further confirmed in the future.

Supplementary Materials: The following supporting information can be downloaded at: <https://www.mdpi.com/article/10.3390/inorganics10120253/s1>, Figure S1: The FTIR spectrum of **1** (green); Figure S2: Comparison of the coordination environments of **1**·g (blue) and **1** (green); Figure S3: PXRD patterns of **1**·g and **1**; Figure S4: Excitation–emission map of **1**; Figure S5: Emission spectra of **1**·g and **1**—excited at 365 nm; Figure S6: Photographs of **1** (a) in 1 bar O₂, (b) air, and (c) a vacuum—excited by 365 nm UV light; Figure S7: The emission spectra of **1**·g in air and 1 atm O₂; Figure S8: Under the excitation of 365 nm, (a) the emission spectra of **1**·g in the temperature range from 80 to 300 K with an interval of 20 K and (b) the integral intensities of **1**·g at different temperatures. Table S1: Elemental analysis results for **1**; Table S2: Crystallographic data and structural refinements of **1**·g and **1**; Table S3: Decay curves of **1** in 1 bar O₂, air, and a vacuum—excited by 375 nm VPL and detected at 542 nm.

Author Contributions: Conceptualization, J.-W.Y.; formal analysis and data curation, W.-T.C., C.-H.L., W.-Q.Z. and J.-T.H.; writing—original draft preparation, L.C. and J.-W.Y.; All authors have read and agreed to the published version of the manuscript.

Funding: This research was funded by National Natural Science Foundation of China (22101211 and 21901189), Municipal Science and Technology Bureau (Jiangke 2021-76).

Institutional Review Board Statement: Not applicable.

Informed Consent Statement: Not applicable.

Data Availability Statement: CCDC 2215582 contains the supplementary crystallographic data for this paper. These data can be obtained free of charge from the Cambridge Crystallographic Data Centre via www.ccdc.cam.ac.uk/data_request/cif (accessed on 6 November 2022).

Conflicts of Interest: The authors declare no conflict of interest.

References

1. Tang, Y.; Wu, H.; Cao, W.; Cui, Y.; Qian, G. Luminescent Metal–Organic Frameworks for White LEDs. *Adv. Opt. Mater.* **2020**, *9*, 2001817. [[CrossRef](#)]
2. Zhang, Q.; Wang, C.F.; Lv, Y.K. Luminescent switch sensors for the detection of biomolecules based on metal-organic frameworks. *Analyst* **2018**, *143*, 4221–4229. [[CrossRef](#)] [[PubMed](#)]
3. Mercuri, G.; Giambastiani, G.; Rossin, A. Thiazole- and Thiadiazole-Based Metal–Organic Frameworks and Coordination Polymers for Luminescent Applications. *Inorganics* **2019**, *7*, 144. [[CrossRef](#)]
4. Chen, L.; Dong, X.-B.; Liao, H.-Y.; Zhang, W.-J.; Mo, Z.-W.; Wang, H.-P.; Ye, J.-W.; Chen, X.-M. Long-Range Rigidity Induced Ultralong Cluster-Centered Phosphorescence. *Chem. Mater.* **2022**, *34*, 9182–9189. [[CrossRef](#)]
5. Wang, X.D.; Wolfbeis, O.S. Optical methods for sensing and imaging oxygen: Materials, spectroscopies and applications. *Chem. Soc. Rev.* **2014**, *43*, 3666–3761. [[PubMed](#)]
6. Mills, A. Oxygen indicators and intelligent inks for packaging food. *Chem. Soc. Rev.* **2005**, *34*, 1003–1011. [[CrossRef](#)]

7. Hei, X.; Zhu, K.; Carignan, G.; Teat, S.J.; Li, M.; Zhang, G.; Bonite, M.; Li, J. Solution-processable copper(I) iodide-based inorganic-organic hybrid semiconductors composed of both coordinate and ionic bonds. *J. Solid State Chem.* **2022**, *314*, 123427. [[CrossRef](#)]
8. Ye, J.-W.; Li, X.-Y.; Zhou, H.-L.; Zhang, J.-P. Optimizing luminescence sensitivity and moisture stability of porous coordination frameworks by varying ligand side groups. *Sci. China Chem.* **2018**, *62*, 341–346. [[CrossRef](#)]
9. Yang, T.; Dai, S.; Tan, H.; Zong, Y.; Liu, Y.; Chen, J.; Zhang, K.; Wu, P.; Zhang, S.; Xu, J.; et al. Mechanism of Photoluminescence in Ag Nanoclusters: Metal-Centered Emission versus Synergistic Effect in Ligand-Centered Emission. *J. Phys. Chem. C* **2019**, *123*, 18638–18645. [[CrossRef](#)]
10. Chen, L.; Dong, X.B.; Mo, Z.W.; Wang, H.P.; Ye, J.W.; Zhang, K.; Chen, X.M. Efficient Restraint of Intra-Cluster Aggregation-Caused Quenching Effect Lighting Room-Temperature Photoluminescence. *Adv. Opt. Mater.* **2021**, *9*, 2100757. [[CrossRef](#)]
11. Lou, X.Y.; Yang, Y.W. Pyridine-Conjugated Pillar[5]arene: From Molecular Crystals of Blue Luminescence to Red-Emissive Coordination Nanocrystals. *J. Am. Chem. Soc.* **2021**, *143*, 11976–11981. [[CrossRef](#)] [[PubMed](#)]
12. Juvenal, F.; Fortin, D.; Harvey, P.D. A Platinum(II) Organometallic Building Block for the Design of Emissive Copper(I) and Silver(I) Coordination Polymers. *Inorg. Chem.* **2020**, *59*, 7117–7134. [[CrossRef](#)] [[PubMed](#)]
13. Wang, S.; Morgan, E.E.; Vishnoi, P.; Mao, L.; Teicher, S.M.L.; Wu, G.; Liu, Q.; Cheetham, A.K.; Seshadri, R. Tunable Luminescence in Hybrid Cu(I) and Ag(I) Iodides. *Inorg. Chem.* **2020**, *59*, 15487–15494. [[CrossRef](#)] [[PubMed](#)]
14. Pander, P.; Sil, A.; Salthouse, R.J.; Harris, C.W.; Walden, M.T.; Yufit, D.S.; Williams, J.A.G.; Dias, F.B. Excimer or aggregate? Near infrared electro- and photoluminescence from multimolecular excited states of N⁺C⁻N-coordinated platinum(ii) complexes. *J. Mater. Chem. C* **2022**, *10*, 15084–15095. [[CrossRef](#)]
15. Gao, X.; Ge, F.; Zheng, H. Improving the Stability and Visualizing the Structural Transformation of the Stimuli-Responsive Metal-Organic Frameworks (MOFs). *Inorg. Chem.* **2020**, *59*, 5093–5098. [[CrossRef](#)]
16. Li, J.; Yuan, S.; Qin, J.S.; Huang, L.; Bose, R.; Pang, J.; Zhang, P.; Xiao, Z.; Tan, K.; Malko, A.V.; et al. Fluorescence Enhancement in the Solid State by Isolating Perylene Fluorophores in Metal-Organic Frameworks. *ACS Appl. Mater. Inter.* **2020**, *12*, 26727–26732. [[CrossRef](#)]
17. Wang, Z.; Huang, X. Luminescent Organic-Inorganic Hybrid Metal Halides: An Emerging Class of Stimuli-Responsive Materials. *Chemistry* **2022**, *28*, e202200609.
18. Dey, A.; Garai, A.; Gude, V.; Biradha, K. Thermochromic, Solvatochromic, and Piezochromic Cd(II) and Zn(II) Coordination Polymers: Detection of Small Molecules by Luminescence Switching from Blue to Green. *Cryst. Growth Des.* **2018**, *18*, 6070–6077. [[CrossRef](#)]
19. Devkota, J.; Kim, K.J.; Ohodnicki, P.R.; Culp, J.T.; Greve, D.W.; Lekse, J.W. Zeolitic imidazolate framework-coated acoustic sensors for room temperature detection of carbon dioxide and methane. *Nanoscale* **2018**, *10*, 8075–8087. [[CrossRef](#)] [[PubMed](#)]
20. Artem'ev, A.V.; Davydova, M.P.; Berezin, A.S.; Samsonenko, D.G. Synthesis and Thermochromic Luminescence of Ag(II) Complexes Based on 4,6-Bis(diphenylphosphino)-Pyrimidine. *Inorganics* **2020**, *8*, 46. [[CrossRef](#)]
21. Cappuccino, C.; Farinella, F.; Braga, D.; Maini, L. Mechanochemistry, an Easy Technique to Boost the Synthesis of CuI Pyrazine Coordination Polymers. *Cryst. Growth Des.* **2019**, *19*, 4395–4403. [[CrossRef](#)]
22. Ki, W.; Hei, X.; Yi, H.T.; Liu, W.; Teat, S.J.; Li, M.; Fang, Y.; Podzorov, V.; Garfunkel, E.; Li, J. Two-Dimensional Copper Iodide-Based Inorganic–Organic Hybrid Semiconductors: Synthesis, Structures, and Optical and Transport Properties. *Chem. Mater.* **2021**, *33*, 5317–5325. [[CrossRef](#)]
23. Zhang, Y.; Yang, Q.; Li, X.; Miao, C.; Hou, Q.; Ai, S. A Cu(i)–I coordination polymer fluorescent chemosensor with amino-rich sites for nitro aromatic compound (NAC) detection in water. *CrystEngComm* **2020**, *22*, 5690–5697. [[CrossRef](#)]
24. Artem'ev, A.V.; Davydova, M.P.; Hei, X.; Rakhmanova, M.I.; Samsonenko, D.G.; Bagryanskaya, I.Y.; Brylev, K.A.; Fedin, V.P.; Chen, J.-S.; Cotlet, M.; et al. Family of Robust and Strongly Luminescent CuI-Based Hybrid Networks Made of Ionic and Dative Bonds. *Chem. Mater.* **2020**, *32*, 10708–10718. [[CrossRef](#)]
25. Li, R.-Z.; Li, D.; Huang, X.-C.; Qi, Z.-Y.; Chen, X.-M. A photoluminescent polymeric chain complex: Synthesis and structure of [(PPh₃)₂Cu₂(μ-I)₂(μ-4,4'-bpy)]_n. *Inorg. Chem. Commun.* **2003**, *6*, 1017–1019. [[CrossRef](#)]
26. Agarwal, R.A. One Dimensional Coordination Polymer of Zn(II) for Developing Multifunctional Nanoparticles. *Sci. Rep.* **2017**, *7*, 13212. [[CrossRef](#)]
27. Vizuet, J.P.; Howlett, T.S.; Lewis, A.L.; Chroust, Z.D.; McCandless, G.T.; Balkus, K.J., Jr. Transition from a 1D Coordination Polymer to a Mixed-Linker Layered MOF. *Inorg. Chem.* **2019**, *58*, 5031–5041. [[CrossRef](#)]
28. Andrzejewski, M.; Katrusiak, A. Piezochromic Porous Metal-Organic Framework. *J. Phys. Chem. Lett.* **2017**, *8*, 279–284. [[CrossRef](#)]
29. Bai, L.; Bose, P.; Gao, Q.; Li, Y.; Ganguly, R.; Zhao, Y. Halogen-Assisted Piezochromic Supramolecular Assemblies for Versatile Haptic Memory. *J. Am. Chem. Soc.* **2017**, *139*, 436–441. [[CrossRef](#)] [[PubMed](#)]
30. Ma, Q.; Zhang, Q.; Yang, M.; Shao, B.; Ouyang, R.; Guo, N. Thermal Quenching Mechanism of Metal-Metal Charge Transfer State Transition Luminescence Based on Double-Band-Gap Modulation. *Inorg. Chem.* **2022**, *61*, 9823–9831. [[CrossRef](#)]
31. Carstea, E.M.; Baker, A.; Bierzoza, M.; Reynolds, D.M.; Bridgeman, J. Characterisation of dissolved organic matter fluorescence properties by PARAFAC analysis and thermal quenching. *Water Res.* **2014**, *61*, 152–161. [[CrossRef](#)]
32. Liao, W.-M.; Li, X.-N.; Zeng, Q.; Zhong, Y.-H.; Yin, Y.-G.; He, J. Enantiomerism, diastereomerism and thermochromism in two Cu₇I₄ cluster-based coordination polymers. *J. Mater. Chem. C* **2019**, *7*, 15136–15140. [[CrossRef](#)]

33. Wang, Z.; Wang, C. Excited State Energy Transfer in Metal-Organic Frameworks. *Adv. Mater.* **2021**, *33*, e2005819. [[CrossRef](#)] [[PubMed](#)]
34. Artem'ev, A.V.; Baranov, A.Y.; Rakhmanova, M.I.; Malysheva, S.F.; Samsonenko, D.G. Copper(i) halide polymers derived from tris[2-(pyridin-2-yl)ethyl]phosphine: Halogen-tunable colorful luminescence spanning from deep blue to green. *N. J. Chem.* **2020**, *44*, 6916–6922. [[CrossRef](#)]
35. López, J.; Murillo, M.; Lifante-Pedrola, G.; Cantelar, E.; Gonzalez-Platas, J.; Rodríguez-Mendoza, U.R.; Amo-Ochoa, P. Multi-stimulus semiconductor Cu(i)–I-pyrimidine coordination polymer with thermo- and mechanochromic sensing. *CrystEngComm* **2022**, *24*, 341–349. [[CrossRef](#)]
36. Liu, S.Y.; Zhou, D.D.; He, C.T.; Liao, P.Q.; Cheng, X.N.; Xu, Y.T.; Ye, J.W.; Zhang, J.P.; Chen, X.M. Flexible, Luminescent Metal-Organic Frameworks Showing Synergistic Solid-Solution Effects on Porosity and Sensitivity. *Angew. Chem. Int. Ed.* **2016**, *55*, 16021–16025. [[CrossRef](#)] [[PubMed](#)]
37. Liu, S.-Y.; Qi, X.-L.; Lin, R.-B.; Cheng, X.-N.; Liao, P.-Q.; Zhang, J.-P.; Chen, X.-M. Porous Cu(I) Triazolate Framework and Derived Hybrid Membrane with Exceptionally High Sensing Efficiency for Gaseous Oxygen. *Adv. Funct. Mater.* **2014**, *24*, 5866–5872. [[CrossRef](#)]
38. Filatov, M.A.; Balushev, S.; Landfester, K. Protection of densely populated excited triplet state ensembles against deactivation by molecular oxygen. *Chem. Soc. Rev.* **2016**, *45*, 4668–4689. [[CrossRef](#)]
39. Li, M.; Cheng, Z.; Wang, X.; Yu, Z.; Zhou, M.; Miao, H.; Zhaxi, W.; Huang, W.; Ma, X.; Chen, Q.; et al. Negative/Zero Thermal Quenching of Luminescence via Electronic Structural Transition in Copper-Iodide Cluster-Based Coordination Networks. *J. Phys. Chem. Lett.* **2021**, *12*, 8237–8245. [[CrossRef](#)] [[PubMed](#)]
40. Liu, B.; Wen, M.-T.; Shen, M.-L.; Miao, W.-N.; He, T.-T.; Xu, L. A new 3D cadmium coordination polymer containing 3-amino-1H-1,2,4-triazole: Synthesis, structure, and property. *Inorg. Chem. Commun.* **2018**, *88*, 38–41. [[CrossRef](#)]
41. Wu, T.; Jiang, S.; Samanta, P.N.; Xie, Y.; Li, J.; Wang, X.; Devashis, M.; Gu, X.; Wang, Y.; Huang, W.; et al. Negative thermal quenching of photoluminescence in a copper-organic framework emitter. *Chem. Commun.* **2020**, *56*, 12057–12060. [[CrossRef](#)] [[PubMed](#)]